

# Scaling and unified characterization of flow instabilities in layered heterogeneous porous media

M. Sajjadi and J. Azaiez

*Department of Chemical and Petroleum Engineering, Schulich School of Engineering, University of Calgary, Calgary, Canada T2N 1N4*

(Received 25 June 2013; published 23 September 2013)

The physics of miscible flow displacements with unfavorable mobility ratios through horizontal layered heterogeneous media is investigated. The flow model is solved numerically, and the effects of various physical parameters such as the injection velocity, diffusion, viscosity, and the heterogeneity length scale and variance are examined. The flow instability is characterized qualitatively through concentration contours as well as quantitatively through the mixing zone length and the breakthrough time. This characterization allowed us to identify four distinct regimes that govern the flow displacement. Furthermore, a scaling of the model resulted in generalized curves of the mixing zone length for any flow scenario in which the first three regimes of diffusion, channeling, and lateral dispersion superpose into a single unifying curve and allowed us to clearly identify the onset of the fourth regime. A critical effective Péclet number  $w_c^*$  based on the layers' width is proposed to identify flows where heterogeneity effects are expected to be important and those where the flow can be safely treated as homogeneous. A similar scaling of the breakthrough time was obtained and allowed us to identify two optimal effective Péclet numbers  $w_{opt}^*$  that result in the longest and shortest breakthrough times for any flow displacement.

DOI: [10.1103/PhysRevE.88.033017](https://doi.org/10.1103/PhysRevE.88.033017)

PACS number(s): 47.20.-k, 47.15.-x, 47.56.+r

## I. INTRODUCTION

The problem of instability in miscible displacements is encountered in a variety of applications such as polymer processing, fixed bed regeneration, and chromatographic separations [1], as well as in oil recovery processes where phase behavior acts in favor of local efficiency of the displacement through miscible flooding. Yet, in many applications, a lower viscosity of the injected solvent results in reduced sweep efficiency of the process due to *viscous instabilities*. Viscous instabilities have been the subject of numerous studies since 1952 when Hill conducted a linear stability analysis along with experiments to examine the coupling between gravity driven and viscous driven instabilities [2]. Interested readers are referred to the reviews of Homsy [3] and McCloud and Maher [4] on viscous fingering in porous media. Other forms of this problem considering the nonmonotonic viscosity profile, non-Newtonian fluids, heat transfer in the system, and the chemical reaction can be found in the literature [5,6].

In field applications, the reservoir rocks have variable permeability and are rarely homogeneous. The nonuniform distribution of the permeability changes the preferred path of the flow and becomes the source of another instability mechanism known as *channeling*. Viscosity and heterogeneity induced instabilities appear in the form of extended tails of the injected fluid, called fingers. The faster these fingers grow, the faster the injected fluid reaches the production end, and the flow is characterized as more unstable. Due to its numerous applications, this problem has been studied extensively by researchers working in different fields varying from geology to chemical and petroleum industries. A large number of investigations have attempted to determine the criteria for the dominance of any of the viscosity or heterogeneity mechanisms in the flow. Such attempts started with quantification of the heterogeneity with a single parameter such as Dykstra-Parson's coefficient  $V_{DP}$  or the Lorenz coefficient  $L_C$  in stratified reservoirs [7] or through geometric parameters for artificially built heterogeneous systems [8,9]. These parameters have mainly considered the range of variations of

permeability and the frequency of these variations to describe the severity of the heterogeneity [10]. In these works, the relative importance of heterogeneity to that of viscous forces traditionally measured through the mobility ratio has been *qualitatively* determined for constant mobility ratios. Koval's method in proposing a single factor  $K = HE$  that combined the effects of heterogeneity  $H$  and viscous forces  $E$  was among the rare quantitative analyses in this regard [11]. Although Koval's factors have been useful in the determination of the loss of efficiency due to both instability mechanisms, it was limited to one-dimensional studies and did not analyze the mechanisms of instability and finger structures. Another quantitative analysis was conducted by Sorbie *et al.* [12] where the  $V_{DP}$  and the correlation length  $l_D$  of random heterogeneity were used as measures of the severity of the heterogeneity. The effects of the ratio of the transverse ( $k_z$ ) to longitudinal ( $k_x$ ) permeability on the flow regimes were investigated using an effective aspect ratio  $R_L = A\sqrt{k_z/k_x}$ , where  $A$  is the geometric aspect ratio. It was found that large values of  $R_L$  corresponding to transverse (vertical) equilibrium (TE) conditions result in dispersive flow, while scenarios far from the TE conditions, namely, in Dykstra-Parson's regimes (DP), result in isolated channeled fingers. However, the effect of  $R_L$  was shown to be important only for very small correlation lengths and became negligible even for  $l_D = 0.1$ . The authors commented that for layered media, transverse permeability may not have significant effects on the flow except for the neutral mobility ratio. In a subsequent study, Yang *et al.* [13] used asymptotic analysis to analyze flows with no dispersion in spatially uncorrelated heterogeneous media for limiting values of the parameter  $R_L$ . The asymptotic analysis was compared with predictions from full numerical simulations and allowed us to separate and characterize the flow in the limiting regimes.

The first experimental study on miscible flows through heterogeneous porous media was performed by Blackwell *et al.* in 1959 [14] and has been a reference for many subsequent analytical and numerical studies. Among these, one should cite the study of Araktingi and Orr [15], who

have used the particle-tracking method to successfully model miscible flows through heterogeneous porous media and have reported results that are in agreement with the experimental ones by Blackwell *et al.* [14]. The pseudospectral method was also used by Tan and Homsy [16] to study the effects of random permeability variations with Gaussian log distribution on viscous fingering. In both studies, the effects of variance and correlation length of the permeability distribution on the growth rate of the instabilities were analyzed. In particular, Araktingi and Orr [15] observed a monotonic increase of the instability with both the correlation length and the variance of the heterogeneity. Tan and Homsy [16] observed a maximum growth rate at a certain correlation length of heterogeneity and discussed the resonance between the mechanisms of instabilities at an optimum correlation length, commensurate with the intrinsic scale of viscous fingers. These two studies were later followed by linear stability analysis and nonlinear simulation studies [1,17–19]. In particular, the study by De Wit and Homsy [1,17], who focused on media with harmonically varying permeability, showed that the wave number at which resonance is observed depends on the log-mobility ratio and the Péclet number.

In this paper, a thorough examination of the effects of different parameters on the development of the instability in heterogeneous media is presented. The study will analyze the different regimes of the flows and will propose a unified picture of the flow that incorporates the effects of all pertinent parameters, including the injection velocity, diffusion rate, and the mobility ratio, as well as the characteristics of the heterogeneous medium such as variance and length scale of permeability.

## II. PHYSICAL MODEL AND NUMERICAL METHOD

Figure 1 shows a schematic of the simplified model used in this work. A fluid (fluid 1) with uniform concentration  $C_1$  is injected in the heterogeneous porous medium with an average velocity  $U$  to displace the resident fluid (fluid 2) of uniform concentration  $C_2$ . The flow is assumed to be incompressible, Newtonian, and isothermal and is governed by the equations

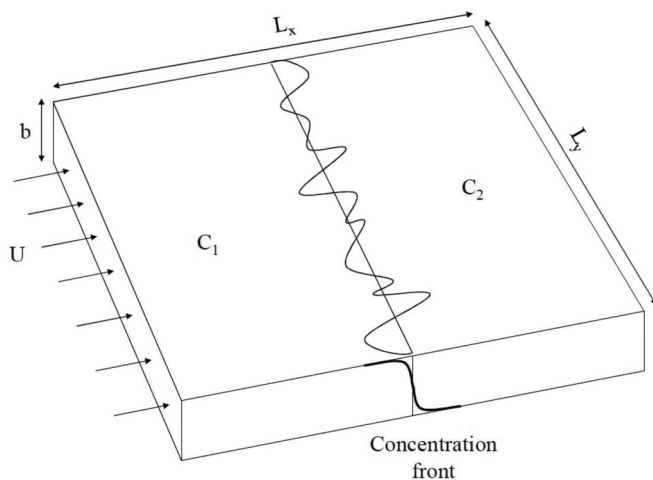


FIG. 1. Schematic of the flow.

for the conservation of mass and momentum and the mass convection-diffusion [20].

$$\frac{\partial u}{\partial x} + \frac{\partial v}{\partial y} = 0, \quad (1)$$

$$\frac{\partial P}{\partial x} = -\frac{\mu\phi u}{k}, \quad (2)$$

$$\frac{\partial P}{\partial y} = -\frac{\mu\phi v}{k}, \quad (3)$$

$$\frac{\partial C}{\partial t} + (\mathbf{u} \cdot \nabla)C = D\nabla^2 C. \quad (3)$$

In the above equations  $\mathbf{u}(u, v)$  is the interstitial velocity vector,  $P$  is the local pressure,  $k$  is local permeability,  $\phi$  is the porosity, and  $\mu$  is the viscosity. Furthermore, the concentration is denoted by  $C$ , and the mass diffusion coefficient is denoted by  $D$ . Following Tan and Homsy [21], diffusive scaling is used to make the equations dimensionless:

$$(\hat{x}, y^*) = \frac{x, y}{D\phi/U}, \quad t^* = \frac{t}{D\phi^2/U^2}, \quad (\hat{u}, v^*) = \frac{(u, v)}{U/\phi}, \quad (4)$$

$$p^* = \frac{P}{D\mu_1\phi/k_1}, \quad \mu^* = \frac{\mu}{\mu_1}, \quad k^* = \frac{k}{k_1}, \quad c^* = \frac{C}{C_1}.$$

The permeability is scaled by the average permeability of the medium  $k_1$ . A Lagrangian reference frame moving with the average injection velocity,  $U/\phi$ , is used so that  $x^* = \hat{x} - t^*$  and  $u^* = \hat{u} - 1$ , and the resulting dimensionless equations are

$$\frac{\partial u^*}{\partial x^*} + \frac{\partial v^*}{\partial y^*} = 0, \quad (5)$$

$$\frac{\partial p^*}{\partial x^*} = -\frac{\mu^*}{k^*}(u^* + 1),$$

$$\frac{\partial p^*}{\partial y^*} = -\frac{\mu^*}{k^*}v^*,$$

$$\frac{\partial c^*}{\partial t^*} + u^* \frac{\partial c^*}{\partial x^*} + v^* \frac{\partial c^*}{\partial y^*} = \left( \frac{\partial^2 c^*}{\partial x^{*2}} + \frac{\partial^2 c^*}{\partial y^{*2}} \right).$$

Henceforth, the asterisks are dropped for simplicity. In the above equations, two variables need to be specified to close the formulation of the problem. First, the nature of the dependence of the viscosity on concentration must be specified. In this study, an exponential dependence of the viscosity on concentration [22–24] is adopted unless otherwise indicated. Such a dependence closely characterizes the “quarter power mixing rule” widely used in the petroleum industry to describe viscosity of nonassociating mixtures and also mixtures of diluted aqueous solutions [25–27]:

$$\mu(c) = \exp[R(1 - c)]. \quad (6)$$

In the above equation  $R$  is the natural logarithm of the viscosity ratio  $\mu_2/\mu_1$  and is related to the mobility ratio  $M$  as  $R = \ln(M)$ . Furthermore, the form of the permeability used to characterize the heterogeneity of the medium needs to be defined. At the pore scale, the variability of the permeability should be negligible for Darcy’s description of the flow to be applicable. But it should be sensed by the flow at a larger scale for the medium to be called heterogeneous. In the present study the permeability of the medium is assumed to vary only in the transverse ( $y$ ) direction. As shall be seen later, the gradient of

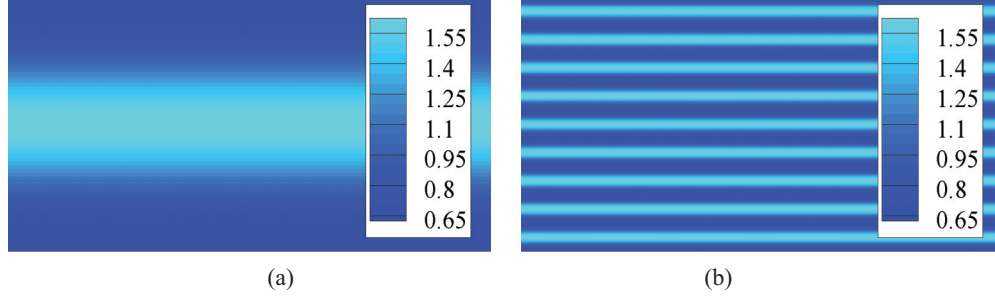


FIG. 2. (Color online) Periodic permeability models with permeability varying between  $k = 0.7$  and  $k = 1.6$  for  $s = 0.5$ ; (a)  $q = 1$  and (b)  $q = 9$ .

the natural log of the permeability  $f = \ln(k)$  appears in the definition of the vorticity, and therefore the heterogeneity will be characterized using the natural log of the permeability  $f$ . For a layered heterogeneous medium,  $f$  is defined as [1]

$$f = \ln[k(x, y)] = s \cos\left(\frac{2\pi}{l_y} qy\right), \quad (7)$$

where  $s$  is the range of variation of  $f$ ,  $q$  is the frequency of layers across the flow channel in the  $y$  direction, and  $l_y$  is the dimensionless width of the domain. Two examples of heterogeneity models for different values of  $q$  are shown in Fig. 2. Although this adopted periodic permeability is a simple model of heterogeneity, it still allows us to reveal some of the mechanisms that can occur in more stochastic permeability models that are difficult to characterize due to the complexity of such models.

Using the definition of vorticity  $\omega$  and the stream function  $\psi$ , where  $\nabla^2\psi = -\omega$ , and adopting the correlations for the viscosity and natural log of the permeability, the set of equations (5) leads to

$$\begin{aligned} \frac{\partial c}{\partial t} + \frac{\partial \psi}{\partial y} \frac{\partial c}{\partial x} - \frac{\partial \psi}{\partial x} \frac{\partial c}{\partial y} &= \nabla^2 c, \quad (8) \\ \omega &= (\nabla \psi + \mathbf{j}) \cdot \left( \frac{d[\ln(\mu)]}{dc} \cdot \nabla c - \nabla \ln k \right) \\ &= -(\nabla \psi + \mathbf{j}) \cdot (R \nabla c + \nabla f). \quad (9) \end{aligned}$$

These dimensionless equations admit a base-state solution  $\bar{c}$  corresponding to a uniform injection velocity (in the moving reference frame;  $\bar{u} = \bar{v} = 0$ ):

$$\bar{c} = \frac{1}{2} \operatorname{erfc}\left(\frac{x}{2\sqrt{t}}\right). \quad (10)$$

The equations are transformed in Hartley space using the Hartley transform [28]. This method has the advantage of increasing the accuracy of differentiations in space but requires periodic boundary conditions. Therefore the solution is sought as the sum of the base-state profile  $\bar{c}$  and perturbations ( $c'$ ) that decay far upstream and downstream [29]. This leads to a nonlinear ordinary differential equation for the concentration perturbation coupled with algebraic equations for the vorticity, all expressed in the Hartley transform space [29]. Since the nonperiodic part of the solution is calculated analytically through base-state equation (10), periodic boundary and initial conditions can be set for the perturbed concentration and for

vorticity as

$$\begin{aligned} (\hat{\omega}, \hat{c})(-\text{Pe}/2 - t, y, t) &= (0, 0), \\ (\hat{\omega}, \hat{c})(\text{Pe}/2 - t, y, t) &= (0, 0), \\ (\hat{\omega}, \hat{c})(x, \text{Pe}/A, t) &= (\hat{\omega}, \hat{c})(x, 0, t), \\ (\hat{\omega}, \hat{c})(x, y, 0) &= (\delta \operatorname{rand}(y) e^{-x^2/\sigma^2}, 0). \end{aligned} \quad (11)$$

In the above equations,  $\text{Pe} = \frac{UL_x}{D}$  is the Péclet number, and  $A = L_x/L_y$  is the aspect ratio of the domain. In dimensionless form  $l_x = \text{Pe}$  and  $l_y = \text{Pe}/A$  are the length and the width of the medium, respectively.

The differential equation for the transform of the concentration perturbation is stepped in time using a fourth-order Adams-Bashforth/Adams-Moulton scheme with operator splitting. Furthermore, underrelaxation was used in the iterative process relating the vorticity to the stream function. This algorithm was shown to be numerically stable and highly accurate for Péclet numbers as high as  $\text{Pe} = 1750$  for log-mobility ratio  $R = 5$  and for  $R$  as large as  $R = 7$  when  $\text{Pe} = 500$ . More details about the numerical algorithm are found in [29,30].

The numerical method was validated by comparing the time evolution and the related viscous finger interactions for the homogeneous case where  $R = 3$ ,  $\text{Pe} = 500$ , and  $A = 2$  with those of Tan and Homsy [21]. Furthermore, the convergence of the numerical solution was examined by considering cases with different spatial resolutions varying from  $256 \times 256$  to  $1024 \times 1024$  while changing the time step accordingly. In particular, for the largest mobility ratio examined,  $R = 5$ , the convergence was confirmed by checking that the concentration contours based on grids of  $512 \times 512$  and  $1024 \times 1024$  were actually identical.

### III. RESULTS AND DISCUSSION

As mentioned before, a heterogeneous medium is characterized by the length scale and variance of the permeability distribution. In the periodic permeability field defined by Eq. (7), the width of the channels, which varies as the inverse of the number of layers, can be regarded as the length scale of heterogeneity, while  $s$  gives a reasonable estimation of the variance of the permeability distribution. In the first stage, the focus will be on the effects of the permeability length scale (number of layers  $q$ ) on the flow structures and growth of the mixing zone. The analysis will then be expanded to analyze the effects of other parameters and examine the flow

breakthrough time. Unless specified otherwise, the mobility ratio, permeability variance, Péclet number, and cell aspect ratio are fixed as  $R = 3$ ,  $s = 0.1$ ,  $Pe = 1024$ , and  $A = 2$ .

**A. Flow structures**

In this section, the results are presented in the form of time sequences of concentration contours which vary between 0 and 1. For brevity, the time sequences are presented not necessarily at the same time intervals, and only the frames that help characterize and explain the development of the flow are shown.

In Fig. 3 two flow displacements through layered media with  $q = 2$  and  $q = 9$  are compared with that in a homogeneous medium. It is clear that the flow structures differ from one case to the other, with the fingers extending faster in the flow direction in the case of the two layers and slower in the nine-layer medium. The number of initial fingers in the heterogeneous cases is determined solely by the number of layers, while it depends on the flow properties ( $Pe, R$ ) in the homogeneous medium. In the latter case, the number of fingers decreases through a number of interaction mechanisms that have already been discussed in the literature. Focusing on the heterogeneous scenarios, the fingers in the two-layered medium remain constrained within the high permeability channels, which is to be contrasted with the nine-layer medium where, from the initial nine fingers, only two end up dominating the flow at later times.

The smaller length scale of heterogeneity in the nine-layer medium results in larger  $\nabla f$  and a rapid growth of instabilities at early times ( $t = 100$ ). However the fingers in the wider channels of the double-layer medium end up surpassing those in the nine-layer medium. This can be explained by the fact that the instability in the double-layer medium is driven by the so-called channeling mechanism in which the dynamics

are governed by the viscous forces and the paths of the flow are dictated by the heterogeneity of the medium [16]. In this case, viscosity and heterogeneity driven forces keep acting with two distinct sharp fingers extending and developing independently until the flow reaches the downstream boundary. In the nine-layer medium however, due to the smaller channel width, after a while the fingers get so close to each other that further development and growth is stalled in favor of lateral dispersion across the channels. This dispersion causes the channeled fingers to fade into a thick wavy front. Since the growth of fingers during this dispersive stage is slow, the thickness of the dispersed front is virtually the same as the length of the fingers at the start of the dispersion. It is anticipated that an even smaller width of the layers will result in an earlier start of dispersion and a thinner dispersed front. Later, instabilities develop at the front as a result of viscous forces, as shown in Fig. 3(c), and lead to two dominant fingers. These instabilities are not dictated by the heterogeneity of the nine-layer medium, but the thickness of the front (influenced by the thickness of the layers) is expected to affect the number of emerging fingers as well as their growth rates.

The differences between the two heterogeneous displacements and the homogeneous one help explain different phenomena observed in experimental and numerical studies of flow through heterogeneous porous media. In particular, the dispersion of fingers across the channels in the nine-layer medium results in stronger mixing of the fluids, which explains the increase in macroscopic dispersion in heterogeneous media reported in different simulation and experimental studies [31,32]. Furthermore, the fact that the effects of heterogeneity in the nine-layer medium pale as the dispersion of fingers across the channels occurs and that the later fingers are not determined by the channels [see Fig. 3(c)] confirms the results of [15], where it was reported that for a smaller correlation

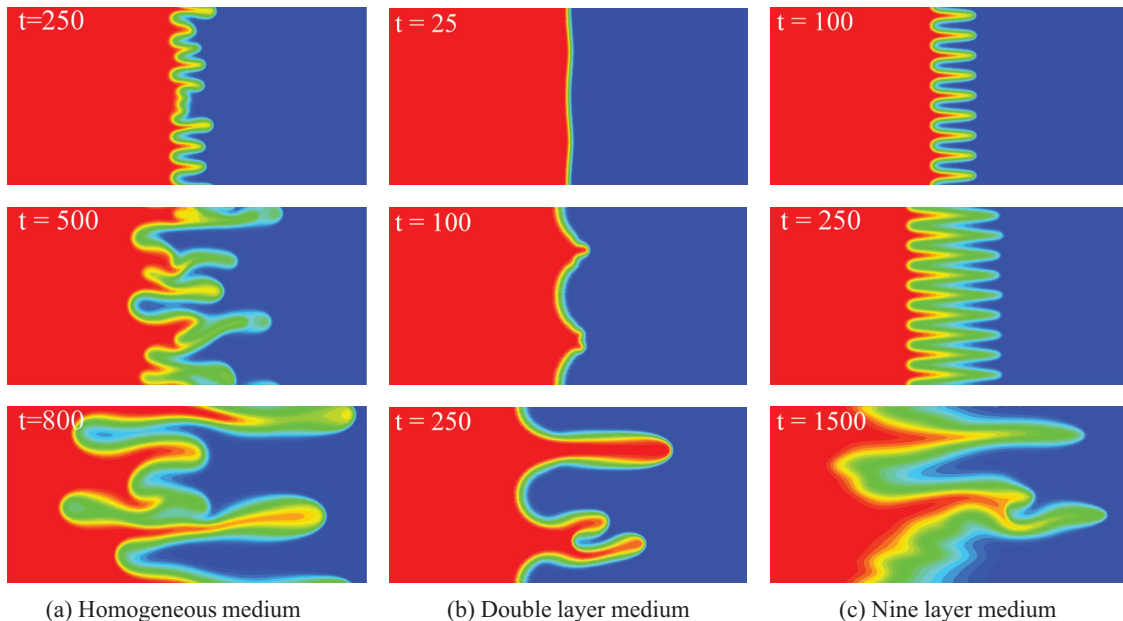


FIG. 3. (Color online) Concentration contours for a viscously unstable flow with  $R = 3$ ,  $Pe = 1024$ , and  $A = 2$  in (a) a homogeneous medium, (b) a double-layer heterogeneous medium, and (c) a nine-layer heterogeneous medium. In each frame the red color (left) represents  $c = 1$ , and the blue color (right) represents  $c = 0$ .

length of heterogeneity, fingers do not follow high permeability channels.

In what follows, the flow instability in heterogeneous media is characterized through a quantitative analysis. *In specie*, the length of the mixing zone along the flow direction [33] and the breakthrough time [18] are used to quantify and characterize the instability.

**B. Mixing length**

By averaging the values of concentration across the flow channel the mixing zone length (MZL) is determined. The mixing zone is defined as the zone with average concentration values between 0.01 and 0.99 [21].

$$c_{av}(x) = \frac{1}{l_y} \int_0^{l_y} c(x,y)dy, \tag{12}$$

$$MZL = x_{c_{av}=0.01} - x_{c_{av}=0.99}.$$

To elaborate more on the behavior of the flow with time, the variation of the MZL with time is depicted in Fig. 4 for the nine-layer case discussed above. For comparison purposes, the MZL of the viscously unstable flow in a homogeneous medium and those of neutral flow ( $R = 0$ ) in the nine-layer medium and in a homogeneous medium are also presented. Figure 4(a) illustrates whole curves in log-log scales to elucidate the trend of the growth of the mixing zone, while Fig. 4(b) focuses on the initial stages of the flow in linear scales.

It can be seen from Fig. 4 that the viscously stable flow ( $R = 0$ ) shows dispersive behavior in both the homogeneous medium and the nine-layer medium, with its MZL growing as  $\sqrt{t}$ . In a homogeneous porous medium, the unstable flow ( $R = 3$ ) goes first through a dispersive regime similar to that observed in the stable flow. This first regime, which lasts up to  $t \simeq 200$ , is followed by the development of viscous instability where MZL grows almost linearly with time [see Fig. 4(b)]. In the nine-layer medium, the unstable flow also goes through initial dispersion, but the MZL graph follows that of the viscously stable flow in the heterogeneous medium, which has a slightly higher dispersion rate than that in the homogeneous medium. Around  $t \simeq 25$ , viscous forces help channeled fingers grow faster than the viscously stable scenario. At this stage,

even though the fingers follow the path dictated by the heterogeneity, their growth rate depends on both viscous forces and heterogeneity. Later, the growth rate of the MZL decreases as the fingers start to disperse across the channels. Lateral dispersion continues until the gradient of concentration across the channels becomes negligible. Subsequently, viscous instabilities develop on the dispersed front at around  $t \simeq 1400$ , and viscous fingering becomes the dominant regime, resulting in a sudden increase of the MZL.

We will now investigate the effect of the length scale of the heterogeneity (width of the channels) on the flow behavior. To this end, more numerical simulations were conducted for various numbers of layers, and the corresponding MZL were determined. Figure 5 depicts the variations of the MZL for the homogeneous medium and for heterogeneous media with  $q = 2, 5, 7, 9$ , and 15. Figure 5 reveals that regardless of the number of layers, the heterogeneous flows go through the same regimes identified earlier in the special case of the nine-layer medium. However, the extent and strength of these regimes vary from one case to the other, and in some cases, such as the two-layer medium, the channeled fingers reach the domain boundary before lateral dispersion of fingers can be actually observed. As can be seen in Fig. 3, the growth rate of the mixing zone is larger at the initial stages of the flow for media for larger number of layers because of larger  $\nabla f$ . Therefore at early times the growth rate of MZL increases monotonically with increasing  $q$ , as shown in Fig. 5(b). At later times, however, a larger number of layers reduces the width of the channels and as a result speeds up lateral dispersion. Therefore the front becomes uniform across the medium faster, and the last stage of viscous fingering develops earlier. As can be seen, the two regimes of channeling and dispersion that precede the viscous fingering are shortened as the number of layers is increased. As we shall see later, for a large enough number of layers, the MZL of the layered heterogeneous medium will actually asymptotically approach that of the homogeneous medium where only the initial diffusive regime and viscous fingering are observed.

**1. Hydrodynamic scaling**

The close similarity in the curves for different numbers of layers raises the question of whether it is possible to obtain a

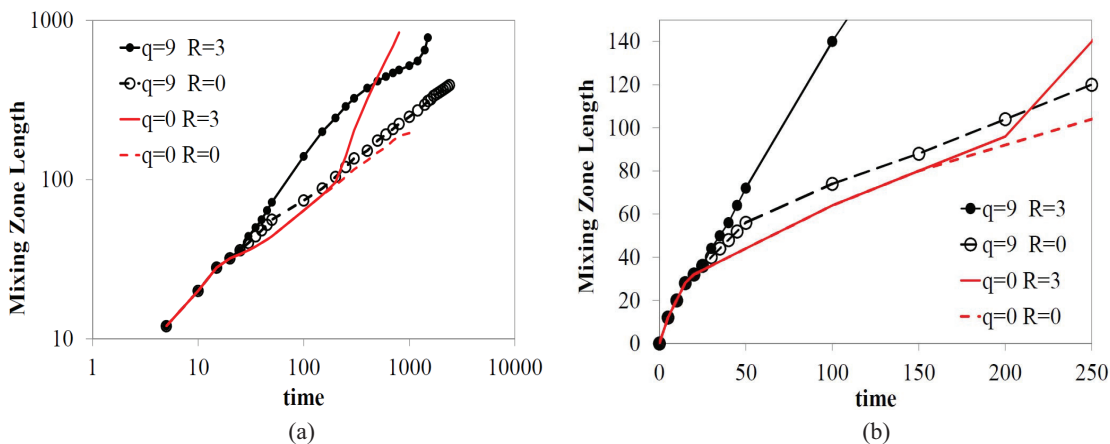


FIG. 4. (Color online) Mixing zone length vs time for stable and unstable flows in a homogeneous medium and in a nine-layer heterogeneous medium;  $Pe = 1024$ ,  $A = 2$ ,  $s = 0.1$ . (a) Throughout the process in logarithmic scales and (b) at early times.

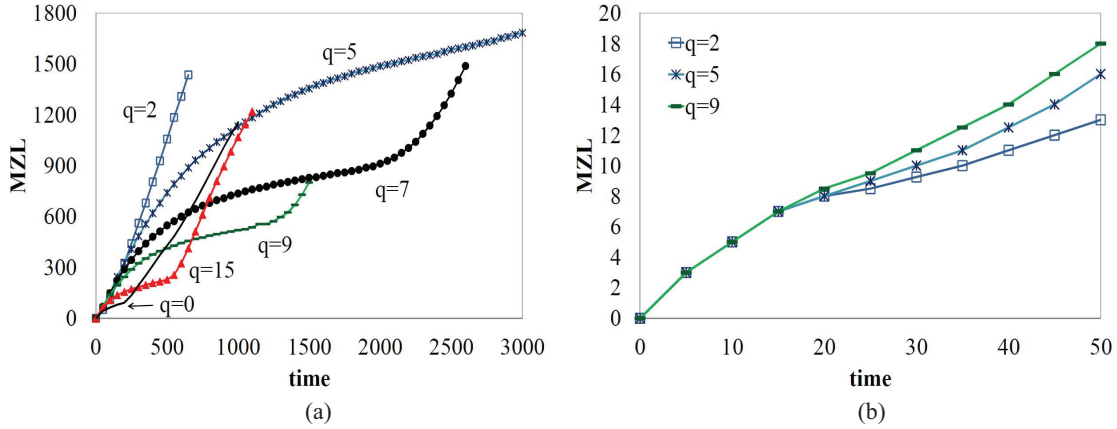


FIG. 5. (Color online) Mixing zone length vs time for heterogeneous media with different numbers of layers for  $R = 3$ ,  $Pe = 1024$ ,  $A = 2$ , and  $s = 0.1$ : (a) throughout the process and (b) at the initial times (fewer graphs are shown for better distinction between the lines).

single curve that can describe the variations of the MZL for any arbitrary number of layers. In order to explore this idea, we propose to analyze the main parameters that govern the flows in the different regimes identified earlier. First, one can note that the first stages of the instability are mainly governed by the flow within the high permeability layers. This suggests characterizing the instability at this scale. Hence a characteristic time for lateral dispersion across a layer of width  $w = L_y/q$  and a characteristic length in the streamwise direction are defined as  $t_c = w^2/D$  and  $x_c = Uw^2/(D\phi)$ , respectively. In dimensionless form these characteristic parameters become

$$t_c^* = \frac{t_c}{D\phi^2/U^2} = \frac{(w^*D\phi/U)^2/D}{D\phi^2/U^2} = w^{*2},$$

$$x_c^* = \frac{x_c}{D\phi/U} = \frac{U(w^*D\phi/U)^2/(D\phi)}{D\phi/U} = w^{*2}.$$

(13)

The asterisks on the dimensionless parameters were retained to distinguish them from the dimensional ones. The width of the domain in dimensionless form is  $l_y = Pe/A$ , and the dimensionless width of each layer can be determined as  $w^* = Pe/(qA)$ . A generalized time  $\tilde{t}$  and length  $\tilde{x}$  are then

defined as

$$\tilde{t} = \frac{t}{t_c} = \frac{t^*}{t_c^*} = \frac{t^*}{\left(\frac{Pe}{qA}\right)^2},$$

$$\tilde{x} = \frac{x}{x_c} = \frac{x^*}{x_c^*} = \frac{x^*}{\left(\frac{Pe}{qA}\right)^2}.$$

(14)

A large number of simulations were conducted for many combinations of a wide range of parameters with  $Pe = 512, 1024, 2048$ ,  $A = 2, 4, 8$ , and  $q = 1$  to 20, and the mixing lengths were determined. The corresponding generalized mixing zone lengths ( $\widetilde{MZL} = MZL/x_c$ ) are plotted versus the generalized time and are shown in Fig. 6(a). It is clear that the scaling does indeed result in a single curve for different displacement scenarios. Even for cases where the simulations stopped due to the fingers reaching the boundaries,  $\widetilde{MZL}$  still follows the unifying generalized curve. However, it should be stressed that the different curves do superpose only up to the time where the viscous fingering regime starts. At this convective regime, the growth rate of the MZL depends on the Péclet number and cannot be predicted based only on this dispersive scaling. The results of this scaling imply that the

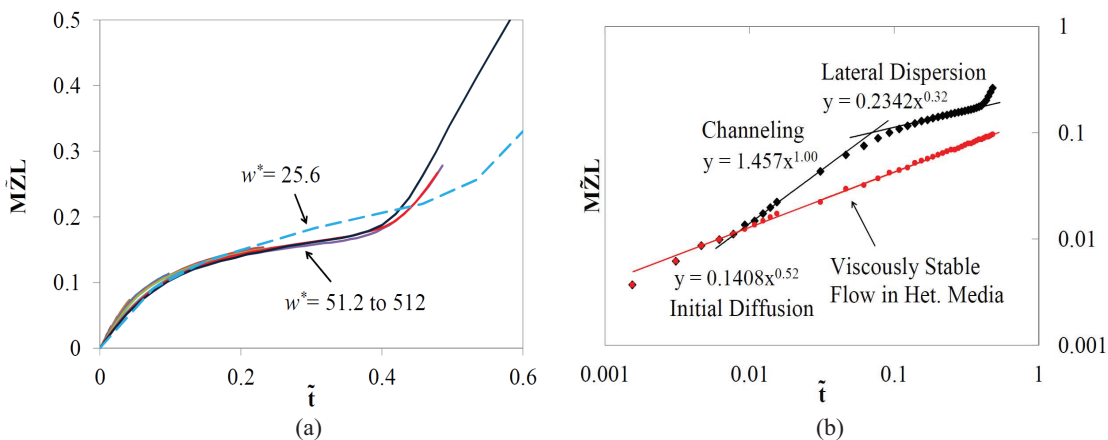


FIG. 6. (Color online) Generalized MZL vs generalized time for  $R = 3$  and  $s = 0.1$  (a) for  $w^* = 25.6, 51.2, 56.9, 64, 73.1, 102.4, 113.8, 128, 146.3, 170.7, 204.8, 256, 241.3,$  and 512 and (b) for  $w^* = 51.2$  in log-log scale, indicating the flow regimes.

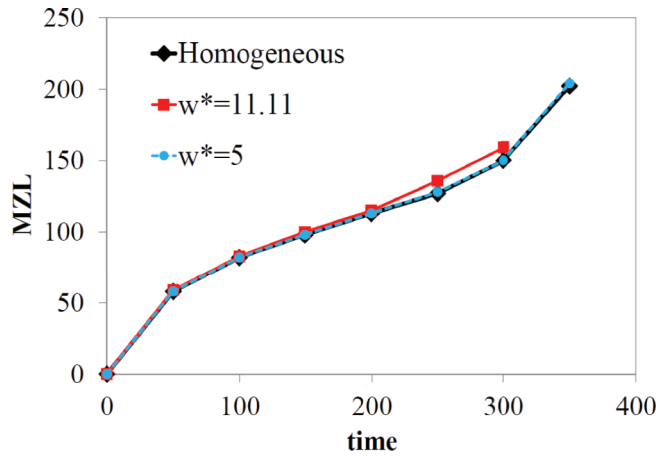


FIG. 7. (Color online) Weak effect of heterogeneity in media with a small dimensionless width of layers for  $R = 3$ ,  $s = 0.1$ ,  $Pe = 200$ , and  $A = 2$ .

quantitative behavior of the displacement can be predicted for any given scenario and length scale of permeability variations.

The proposed generalization allows identifying and defining the different dominant flow regimes and the transition times in between these regimes. Figure 6(b) shows a log-log plot of  $\widetilde{MZL}$  versus  $\tilde{t}$  with trend lines fit to each segment categorizing a particular flow regime. These regimes can be identified as *initial diffusion*, *channeling*, *lateral dispersion*, and *viscous fingering*. In the initial diffusion regime,  $\widetilde{MZL}$  grows almost as  $\sqrt{\tilde{t}}$ . The coupling between viscous forces and heterogeneity increases the growth rate of  $\widetilde{MZL}$  to almost a linear function of time,  $\tilde{t}^{1.01}$ , and leads to the channeling regime. In the third regime, lateral dispersion causes the growth rate to decrease to less than the initial diffusion regime and  $\widetilde{MZL} \equiv \tilde{t}^{0.32}$ . Ultimately, viscous fingering leads to  $\widetilde{MZL}$  growing faster than in previous regimes. The transition from initial diffusion to channeling occurs at  $\tilde{t}_{dc} \approx 0.01$ , while that from channeling to lateral dispersion is at  $\tilde{t}_{cd} \approx 0.07$ . Finally, lateral dispersion leads to viscous fingering, which develops at different times depending on the value of  $Pe$ .

The scaling group  $w^* = Pe/(qA) = Uw/D$  suggests that larger velocity, weaker diffusion rate, or larger channel width results in a slower transition from channeling to lateral dispersion and further to viscous fingering. In all these cases, fingers develop individually in the channels and grow longer with minimum interactions. Such fingers require more time

to get transversely dispersed, and the flow stays in the lateral dispersion regime for a longer time before viscous fingering starts.

Small values of  $w^*$ , however, result in stronger dispersion compared to the rate of advancement of instabilities and hinders the development of channeling. In such cases, emerging channeling fingers, if any, will fade rapidly into a dispersed front in the early stages of the flow, allowing viscous fingering to develop across that front. In an extreme case, a layered system with a large enough number of layers will not experience channeling or lateral dispersion and will go directly through viscous fingering as in a homogeneous porous medium. Therefore as  $w^*$  decreases,  $\widetilde{MZL}$  deviates from the unifying generalized curve characterizing the flow in a heterogeneous medium, and as we shall see later,  $\widetilde{MZL}$  will approach that of a homogeneous case. One can therefore select a critical value of the effective Péclet number  $w_c^*$  to separate flows in which heterogeneity is dominant from those in which it can be ignored. The value of this critical Péclet number can be determined on the basis of the extent of the lateral dispersion regime and, specifically, the slope of the  $\widetilde{MZL}$  in that region. Hence a displacement flow with a  $\widetilde{MZL}$  slope in the lateral dispersion region of more than about  $\tilde{t}^{0.4}$  (the slope of the lateral dispersion regime on the curve corresponding to  $w^* = 25.6$ ) leans towards a homogeneous system, and the effects of heterogeneity can be deemed negligible.

To further illustrate these conclusions, the MZL for  $Pe/(qA) = 11.11$  and for  $Pe/(qA) = 5$  as well as for the homogeneous medium are depicted in Fig. 7. The results are presented in terms of MZL since  $\widetilde{MZL}$  is not defined for a homogeneous medium. It is clear that the curves are virtually indistinguishable, indicating that flows in such heterogeneous media essentially behave like that in a homogeneous medium, at least in terms of their MZL.

The close similarity between heterogeneous flows with small effective Péclet number  $w^*$  and those in a homogeneous medium was actually found not to be limited to quantitative properties such as the MZL and is also observed in the actual flow structures. Figure 8 shows concentration contours for the homogeneous medium and heterogeneous media with  $w^* = 11.11$  and  $w^* = 33.3$  at  $t = 300$ . It is clear that the flow structures in the homogeneous medium and the heterogeneous one with  $w^* = 11.11$  are virtually identical, while the effects of heterogeneity manifesting in the form of fingers developing in the high permeability channels are dominant in the medium with  $w^* = 33.3$ . This further confirms the criteria based on

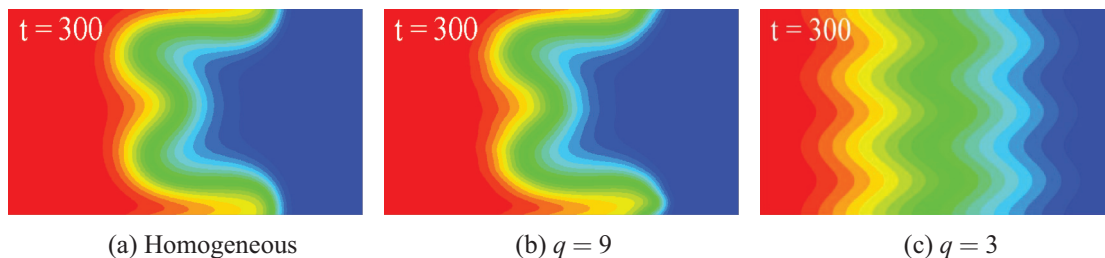


FIG. 8. (Color online) Concentration contours for  $R = 3$ ,  $Pe = 200$ ,  $A = 2$  for (a) a homogeneous porous medium and (b) nine-layer heterogeneity, with  $w^* = 11.1$ , and (c) three-layer heterogeneity, with  $w^* = 33.3$ . In each frame the red color (left) represents  $c = 1$ , and the blue color (right) represents  $c = 0$ .

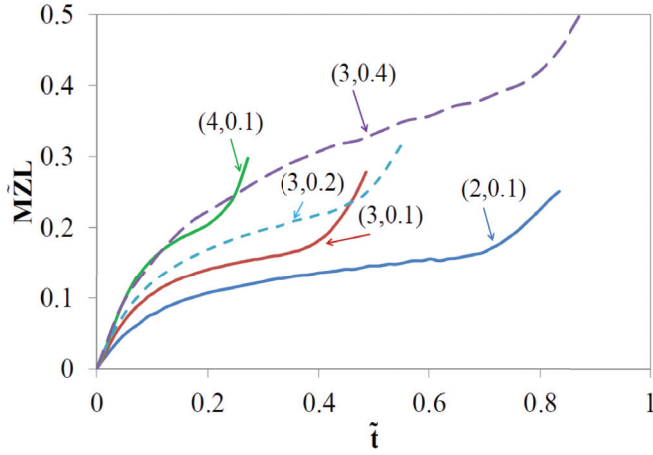


FIG. 9. (Color online) Generalized MZL for different combinations of mobility ratio and variance of permeability distribution  $(R, s)$ .

the parameter  $w^*$  to define a limit for a permeability length scale below which the effects of heterogeneity are so small that they do not play any significant role in driving the instabilities, and the medium can be treated as homogeneous in terms of the flow dynamics. As a general guideline, one may treat flow displacements in heterogeneous media as effectively homogeneous flows for  $w^* < w_{c-H}^* = 15$  and as heterogeneous flows for  $w^* > w_{c-H}^* = 30$ .

It is important at this stage to note that the generalized curve in Fig. 6(b) was generated for given values of the log-mobility ratio ( $R = 3$ ) and permeability variance ( $s = 0.1$ ). It would therefore be interesting to determine how the previous conclusions may change for other values of  $R$  and  $s$ .

Figure 9 depicts generalized curves for different combinations of  $(R, s)$ . Regardless of the values of  $R$  or  $s$ , all curves follow the same trends and go through the different regimes that have been identified earlier. It is worth noting that increasing  $s$  has the same effect on  $\widetilde{MZL}$  as decreasing  $q$  had on MZL in Fig. 5. Higher permeability variance leads to stronger growth rate of fingers inside the channels during the channeling regime, while it delays the transition to viscous fingering. This is different from the effect of the viscosity ratio,

which shortens the transition regime as it increases the growth rate of instabilities in all regimes.

Based on the results in Fig. 9 one may wonder if the scaling developed so far can be further extended to include the effects of the heterogeneity variance and viscosity. These two aspects are examined in the following sections.

### 2. Heterogeneity scaling

A proper scaling of MZL to account for the effects of changes in the permeability variance can be accomplished by dividing both the generalized length and time by  $k_c = \exp(2s)$ , which is the ratio between the maximum and minimum permeability values. This scaling can be justified by noting from Darcy's equation that the effects of permeability  $k$  are commensurate with those of velocity  $u$ , *ceteris paribus*:

$$u = -\frac{k}{\mu} \frac{\partial p}{\partial x}. \tag{15}$$

One may therefore posit that variations of  $k \equiv e^s$  affect MZL in the same way as velocity does, or, equivalently, as  $Pe = UL_x/D \equiv w^*$ . This and the fact that we have seen that the appropriate hydrodynamic scaling is based on  $w^{*2}$  lead to the proposed heterogeneity scaling of  $e^{2s}$  commensurate with  $w^{*2}$ . The results of scaling the generalized MZL to account for the effect of the strength of heterogeneity as  $\tilde{t}_s = \tilde{t}/e^{2s}$  and  $\widetilde{MZL}_s = \widetilde{MZL}/e^{2s}$  are shown in Fig. 10. It is clear that the proposed scaling does allow us to collapse the various curves into a single unifying curve that allows us to characterize MZL regardless of the values of the heterogeneity variance. Figure 10(b) shows the renormalized curves for different log-viscosity ratios, and here again qualitative similarity between the different curves indicates that it may be possible to also scale the effects of viscosity.

### 3. Viscosity scaling

As mentioned before, the effect of the log-mobility ratio is to enhance the instabilities in all regimes, and it is different from the effect of other properties discussed so far, which are mainly related to the heterogeneity of the medium. The graphs of  $\widetilde{MZL}_s$  for different values of  $R$  shown in Fig. 10(b) can be

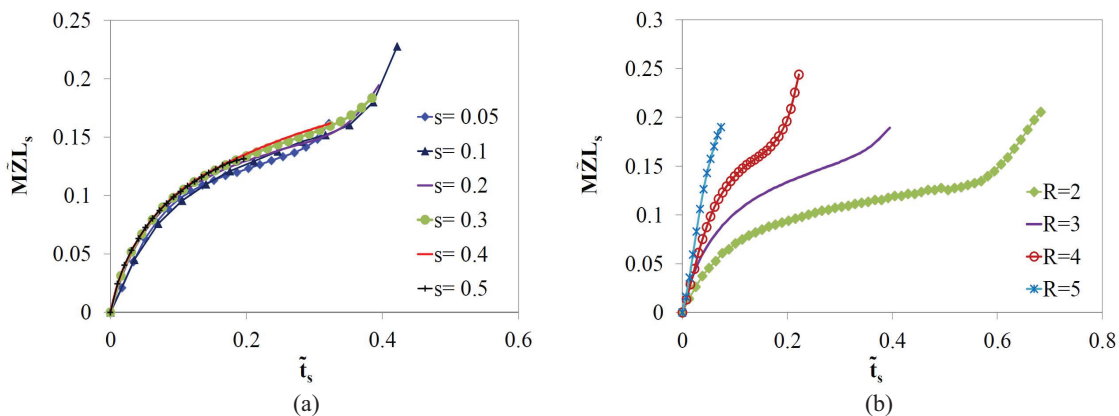


FIG. 10. (Color online) Renormalization of MZL to account for variance of permeability distribution  $s$ . The flow parameters are  $Pe = 2048$ ,  $A = 4$ ,  $q = 7$ , (a)  $R = 3$ , and (b)  $s = 0.1$  for different log-mobility ratios.

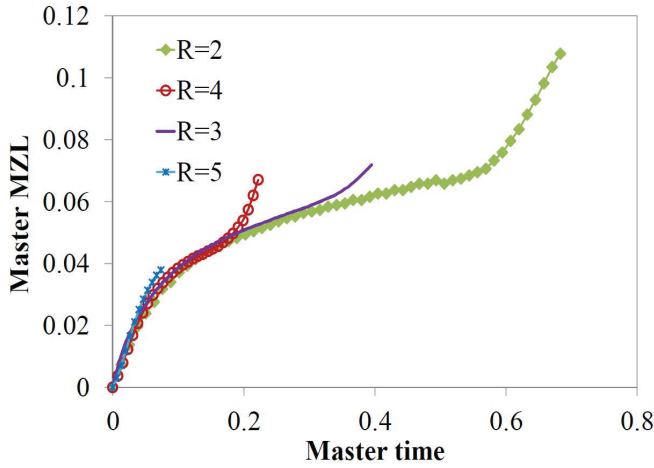


FIG. 11. (Color online) Fitting of  $\widetilde{MZL}_s$  curves of different displacement scenarios with  $Pe = 2048$ ,  $A = 4$ ,  $q = 7$ , and  $s = 0.1$  and for different mobility ratios, as noted on the plot.

reduced to a master curve by scaling only the length by  $e^{R/3.1}$ . Hence the proposed scaling is as follows:

$$MZL_{\text{master}} = \frac{\widetilde{MZL}_s}{e^{(R/3.1)}}, \quad t_{\text{master}} = \tilde{t}_s. \quad (16)$$

This normalization was obtained through an estimation of the calculated factors for matching the curves and is not based on any actual physical arguments. Still, as can be seen from Fig. 11, it allowed us to build a general unifying curve that characterizes the first flow regimes for any values of the fluid properties or the medium's heterogeneity. Note that despite the superposition of the curves in the channeling and lateral dispersion regimes, earlier transition from lateral dispersion to viscous fingering is observed for higher log-mobility ratios.

Before closing this section, the dependence of the previous conclusions on the type of viscosity model will be examined. Different models are used in the literature [34,35], but for the sake of brevity, our discussion will be based on the quarter power mixing rule defined as [35]

$$\left(\frac{1}{\mu}\right)^{1/4} = \left(\frac{C_1}{\mu_1}\right)^{1/4} + \left(\frac{C_2}{\mu_2}\right)^{1/4}. \quad (17)$$

Generalized MZL plots generated with the quarter power mixing rule are shown in Fig. 12 for a viscosity ratio of  $M = 20$  equivalent to  $R = 3$  in the exponential viscosity correlation for  $q = 5$  and  $q = 7$ . For comparison purposes, the corresponding  $\widetilde{MZL}$  curves for the exponential viscosity model are also plotted. It can be seen that the variations of  $\widetilde{MZL}$  of both viscosity models are qualitatively similar, and the different regimes discussed earlier can be identified in both cases. This implies that the same conclusions can be drawn for both models and indicates that the scaling scheme may actually be valid for any viscosity model.

### C. Time-dependent dominance of flow regimes

The present study shows that flows in heterogeneous porous media go through the same flow regimes at different

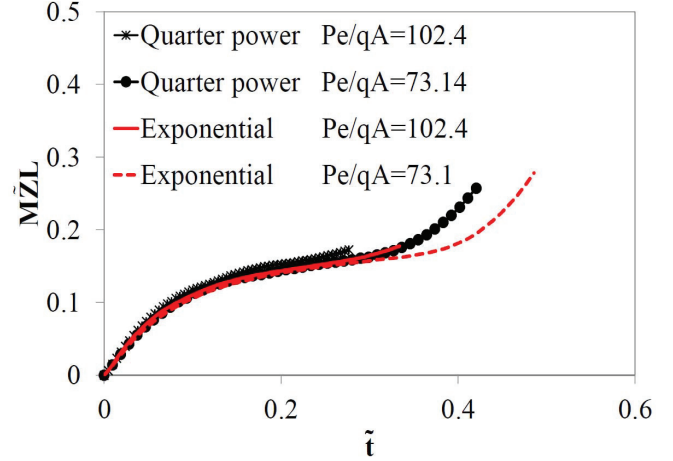


FIG. 12. (Color online) Effect of the viscosity model on MZL for an unstable flow with a mobility ratio of  $M = 20$  corresponding to  $R = 3$ , with  $Pe = 2048$ ,  $A = 4$ , and  $s = 0.1$  in a five-layer and a seven-layer medium corresponding to  $w^* = 102.4$  and  $w^* = 73.1$ , respectively.

heterogeneity length scales and with different flow properties. Therefore the dominance of any instability mechanism depends on the time window at which it is considered, and this allows us to explain and predict the flow behavior. In particular, the dominance of heterogeneity induced instabilities in the large length scale of heterogeneity reported by [15,36] is due to the fact that the effective Péclet number  $Pe/(qA)$  in such cases is large, and as a result the flow will be mainly in the channeling regime on the generalized graph. Furthermore, in the work of Tan and Homsy [16] followed by that of De Wit and Homsy [17], the average slope of MZL between  $t = 200$  and  $t = 400$ ,  $\dot{L}_d$ , was used to characterize the instability. Their simulations showed that  $\dot{L}_d$  has a maximum at a particular heterogeneity length scale, which was attributed to a resonance between viscosity and heterogeneity driven instabilities at commensurate length scales. The results of the present study and the identified general flow behavior show that such a maximum can be attributed to the fact that in a heterogeneous medium,  $\dot{L}_d$  increases with  $q$  because of higher  $\nabla f$  for larger  $q$ , hence the initial increase. However, for even larger  $q$ , the flow goes through lateral dispersion, therefore leading to smaller average  $\dot{L}_d$ , for a fixed time period. Figure 13 depicts  $\dot{L}_d$  determined between  $t = 200$  and  $t = 400$  versus the number of layers for the same conditions used by [17] ( $R = 3$ ,  $Pe = 2048$ ,  $A = 2$ ). If the same displacement process is considered at later times (e.g., between  $t = 600$  and  $t = 1000$ , as shown in Fig. 13), heterogeneity models with larger length scales get the chance to go through lateral dispersion, and one observes a rapid decrease in the average slope of MZL. The slope of MZL increases with time in the channeling regime; hence for media in which the flow is still in the channeling regime an increase in  $\dot{L}_d$  is expected at the  $t = 600$  to  $t = 1000$  time window. Due to these changes, it is not surprising that the maximum  $\dot{L}_d$  shifts from  $q = 6$  to a smaller value of  $q$  as the time window is changed from  $[t = 200, t = 400]$  to  $[t = 600, t = 1000]$ .

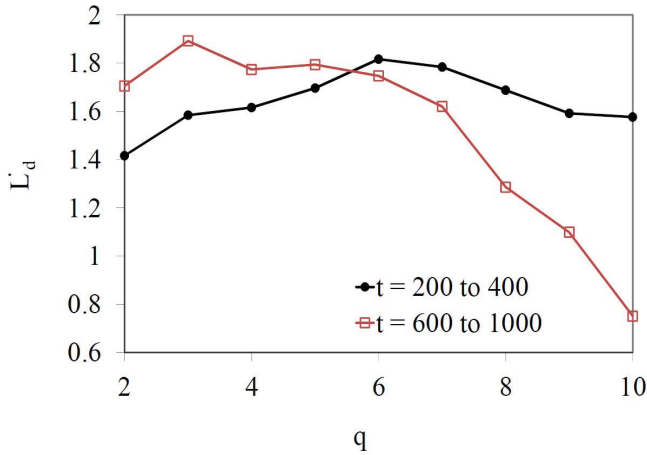


FIG. 13. (Color online) Average slope of MZL  $\bar{L}_d$  at different time windows for  $R = 3$ ,  $Pe = 2048$ ,  $A = 2$ , and  $s = 0.01$ .

**D. Breakthrough time**

Beside the mixing zone length, there are other parameters for quantifying the instability that are easier to measure in field applications. One of these parameters is the breakthrough time of the injected solvent at the production end. The breakthrough time (BT) is defined as the time when the leading edge of the mixing zone ( $c = 0.01$ ) reaches the downstream end of the porous medium with the total length  $L_{total} = t_{BT} + x_{c=0.01}$  at BT. In this section the effect of the length scale of the permeability on the breakthrough time is analyzed, and the applicability of the discussed generalization to such measurements is sought.

Figure 14(a) depicts the variation of the BT with the number of layers  $q$  for the sets  $(Pe, A) = (3072, 8), (2048, 4), (2048, 2)$ , and  $(1024, 2)$ . All results were obtained for  $R = 3$  and  $s = 0.1$ , and the point  $q = 0$  corresponds to the homogeneous case. It is clear that the variation of BT with  $q$  is nonmonotonic and actually exhibits a minimum and a maximum for all considered cases. For wide channels (small but nonzero  $q$ ), the flow is more unstable since it is dominated by channeling where fingers develop early, particularly in comparison with the homogeneous case ( $q = 0$ ; cf. Fig. 3), hence the smaller breakthrough time. This minimum breakthrough time

corresponds to the largest number of layers for which the flow remains in the channeling regime throughout the displacement process. For intermediate values of  $q$ , the flow spends most of its traveling time in the lateral dispersion regime, resulting in longer breakthrough times, while for narrow channels (large  $q$ ), a fast transition to viscous fingering causes early breakthrough of the injected fluid. Clearly, there are two optimum numbers of layers,  $q_{optM}$  and  $q_{optm}$ , that result in a maximum and a minimum breakthrough time. These optimum numbers of channels depend on the Péclet number and the cell aspect ratio and seem to decrease with increasing  $A$  and decreasing  $Pe$ .

Following the scaling strategy adopted for characterizing the flow through MZL, the BT is plotted versus  $1/w^*$ , and the results are shown in Fig. 14(b). The scaling clearly allows us to superpose all curves into a single one regardless of the combinations of  $Pe$  and  $A$  and to distinguish the extrema of BT. In particular, it is found that the minimum of the breakthrough time is reached for  $w^* = w_{optm}^* \approx 250$ , while the maximum is attained for  $w^* = w_{optM}^* \approx 60$ . It can be concluded that for any displacement scenario (a given mobility ratio and a diffusion rate) in a porous medium with determined permeability distribution, the injection rate of the solvent can be adjusted to the distance between injection and production locations to meet the optimum characteristics  $\frac{Pe}{qA}$ . This will ensure that the process remains in the lateral dispersion regime for most of the time and promotes high sweep efficiency of the process.

**E. Effects of dispersion**

The previous scaling and flow analysis was based on constant isotropic diffusion in the flow. Questions may, however, arise about the extent and validity of the present study for general dispersive flows. In the case of homogeneous media, a number of numerical studies have examined the effects of dispersion on the dynamics of viscous fingering [16,37–39]. It was found that *isotropic* velocity-dependent dispersion has no significant effects on the finger structures and quantitative properties such as the mixing length, while anisotropy can result in important differences in the finger structures. For heterogeneous media, the picture becomes more complicated as a result of the competition between

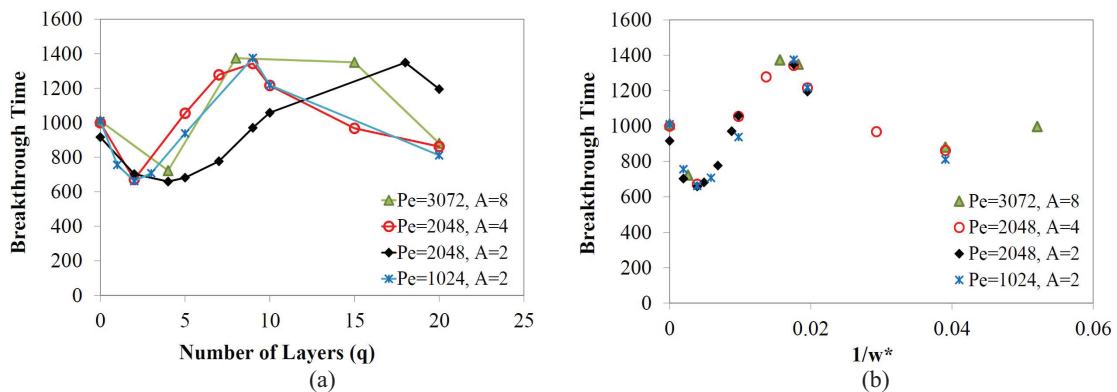


FIG. 14. (Color online) Breakthrough time of the flow with  $R = 3$ ,  $s = 0.1$  at the total dimensionless length of  $L_{total} = 2700$ ; (a) breakthrough time vs the number of layers for different  $Pe$  and  $A$  and b) breakthrough time vs  $1/w^* = qA/Pe$ .

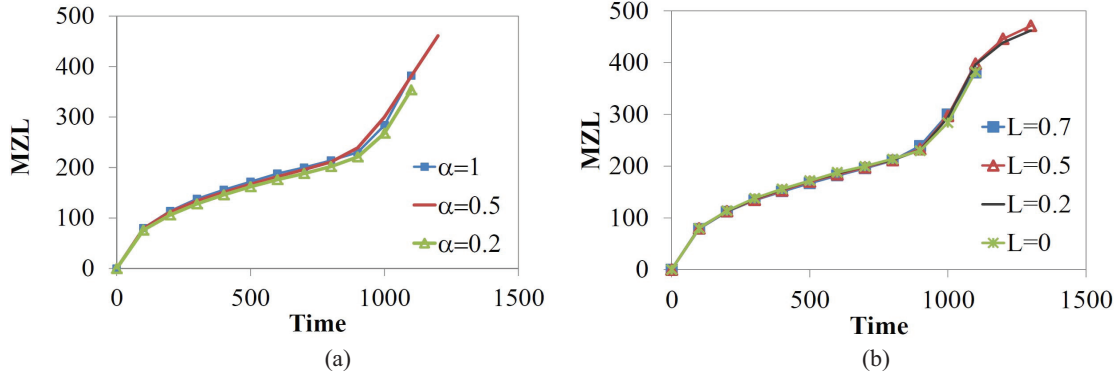


FIG. 15. (Color online) Effect of dispersion on MZL for  $s = 0.1, q = 9, R = 2, Pe = 512$ , and  $A = 2$  for (a)  $L = 0.7$  and different  $\alpha$  and (b)  $\alpha = 0.5$  and different  $L$ .

different mechanisms [40]. The present study revealed that all flows dominated by the medium heterogeneity ( $w^* > w_{c-H}^*$ ) can be characterized by a single generalized curve. For such flows, it is reasonable to expect that the effects of dispersion will be negligible in comparison with those arising from the medium heterogeneity, and actually, most relevant studies have ignored dispersive effects [12,13]. In order to ascertain this and check the generality of the proposed scaling, simulations that account for dispersion were carried out for layered heterogeneous media using a velocity-dependent anisotropic dispersion model [38,41]. Two dimensionless groups are adopted:  $\alpha = \frac{a_T}{a_L}$ , which represents the ratio of the strength of dispersion in the transverse and longitudinal directions, and  $L = \frac{a_L U}{a_L U + D}$ , which measures the relative strength of the longitudinal dispersion [38].

A series of simulations was conducted to determine the effects of parameters  $\alpha$  and  $L$ . It was found that for flows dominated by heterogeneity, velocity-dependent anisotropic dispersion has very small effects on the finger structures and quantitative properties such as the mixing length. Actually, the only noticeable effects were in the fourth regimes, where some minor differences in the fingers' shapes were observed, although the overall structure and number of fingers were unaffected by dispersion.

Figure 15 depicts the variation of the MZL with time for different values of the dispersivity ratio  $\alpha$  and strength  $L$  and for  $A = 2, s = 0.1, q = 9, Pe = 512$ , and  $R = 2$ . Clearly, the mixing zone length is not affected by dispersion over the wide range of parameters  $\alpha$  and  $L$  that has been explored. Results were also obtained for other values of  $A, s, Pe$ , and  $R$ , and it was found that in all cases the MZL does not change as a result of dispersion, at least in the first three regimes, while some differences may be observed during the last fingering regime. These results indicate that the proposed scaling actually extends to dispersive flows and that the previous conclusions are valid for general dispersive flows in layered heterogeneous media.

#### IV. SUMMARY AND CONCLUSION

The coupling between viscous fingering and heterogeneity induced instability has been investigated through a qualitative analysis of concentration contours as well as quantitative

characterizations through the mixing zone length and the breakthrough time. The study considered a wide range of parameters such as the Péclet number, cell aspect ratio, fluid mobility ratio, and heterogeneity length scale and variance and revealed that, in all the scenarios examined, flow displacements in layered heterogeneous media go through similar flow regimes, although not necessarily at the same extent and with the same intensity. Generalized curves have been obtained for different combinations of the mobility ratio and the variance of the permeability distribution by scaling time and MZL using characteristic time and characteristic length based on the channel width. The slopes of the generalized curve have been used to identify four regimes that the flow goes through, namely, an initial diffusive regime followed by a channeling regime, then lateral dispersion, and, finally, viscous fingering. Such characterization of the flow regimes helps to explain the dominance of viscous fingering or channeling regimes reported in earlier studies for different length scales of permeability and for different Péclet numbers. Furthermore, this scaling allowed us to identify the transition from flows where heterogeneous effects are dominant to those where these effects can be neglected and the flow can be treated as homogeneous. Such a transition is governed by a critical effective Péclet number based on the channels width  $w_c^*$ , whose value depends on the viscosity ratio and the strength of heterogeneity. Moreover, it is shown that for small values of the effective Péclet number, the qualitative behavior and structure of the flows are virtually identical to those of the homogeneous case. These results and the scaling obtained in the case of diffusive flows were found to be also valid when an anisotropic velocity-dependent dispersion is considered. The scaling of MZL was further extended to account for the effects of the mobility ratio and permeability variance and led to a general master curve that can be used to characterize quantitatively any flow in layered heterogeneous media. Such master curves allow us to superpose the MZL up to the viscous fingering regime and allows us to identify clearly the start of this last regime.

The flow was also characterized in terms of the breakthrough time. It was found that the variation of BT with the number of layers  $q$  is nonmonotonic and goes through a minimum for small values of the number of layers  $q$  and a maximum for intermediate values. Media with a large

number of layers lead to the same BT as the homogeneous medium. Two optimal values of the effective Péclet number  $w_{\text{opt}}^*$  that lead to a maximum and a minimum value of BT were determined. Here too these optimal values are expected to depend on the permeability variance and fluid viscosity ratios and the total length of the domain.

The present study has focused on the viscous fingering instability in isothermal miscible displacements. However, it is expected that similar characterizations can be extended to other displacements such as in Rayleigh-Taylor (gravity driven) instability [31,42] or thermoviscous fingering [43] and would help to explain observed phenomena such as the resonance between the driving mechanisms of instability [42] or the

dominance of any of the mechanisms at different length scales [31,43]. Furthermore, similarity in the behavior of the mixing zone for different heterogeneous media has also been reported for immiscible displacements [44], and it is presumable that the present scaling approach can also be adopted to characterize the flow behavior in immiscible flows.

#### ACKNOWLEDGMENTS

The authors would like to acknowledge the support of Alberta Innovates-Technology Futures and the Natural Sciences and Engineering Research Council of Canada (NSERC) and the use of the computing resources of the WestGrid cluster.

- 
- [1] A. De Wit and G. Homsy, *J. Chem. Phys.* **107**, 9609 (1997).
  - [2] S. A. Hill, *Chem. Eng. Sci.* **1**, 247 (1952).
  - [3] G. Homsy, *Annu. Rev. Fluid Mech.* **19**, 271 (1987).
  - [4] K. McCloud and J. Maher, *Phys. Rep.* **260**, 139 (1995).
  - [5] O. Manickam and G. Homsy, *Phys. Fluids* **6**, 95 (1994).
  - [6] S. Hejazi, P. Trevelyan, J. Azaiez, and A. De Wit, *J. Fluid Mech.* **652**, 501 (2010).
  - [7] J. L. Jensen and L. W. Lake, *SPE Reservoir Eng.* **3**, 629 (1988).
  - [8] M. Ferer, K. Stevenson, G. Bromhal, J. Gump, J. Wilder, and D. Smith, *Phys. A* **367**, 7 (2006).
  - [9] H. Siddiqui and M. Sahimi, *Chem. Eng. Sci.* **45**, 163 (1990).
  - [10] J. E. Warren and H. S. Price, *SPE Journal* **1**, 153 (1961).
  - [11] E. J. Koval, *SPE Journal* **3**, 145 (1963).
  - [12] K. Sorbie, F. Feghi, G. Pickup, P. Ringrose, and J. Jensen, *SPE Adv. Technol. Ser.* **2**, 78 (1994).
  - [13] Z. Yang, Y. Yortsos, and D. Salin, *Adv. Water Resour.* **25**, 885 (2002).
  - [14] R. Blackwell, J. Rayne, and W. Terry, *J. Pet. Technol.* **10**, 1 (1959).
  - [15] U. G. Araktingi and F. M. Orr, Jr., *SPE Advanced Technology Series* **1**, 71 (1993).
  - [16] C.-T. Tan and G. Homsy, *Phys. Fluids A* **4**, 1099 (1992).
  - [17] A. De Wit and G. Homsy, *J. Chem. Phys.* **107**, 9619 (1997).
  - [18] C.-Y. Chen and E. Meiburg, *J. Fluid Mech.* **371**, 269 (1998).
  - [19] A. Riaz and E. Meiburg, *J. Fluid Mech.* **517**, 1 (2004).
  - [20] M. Islam and J. Azaiez, *Transp. Porous Media* **84**, 821 (2010).
  - [21] C. Tan and G. Homsy, *Phys. Fluids* **31**, 1330 (1988).
  - [22] D. Pritchard, *J. Fluid Mech.* **508**, 133 (2004).
  - [23] M. Islam, J. Azaiez, and B. Maini, *Comput. Therm. Sci.* **2**, 183 (2010).
  - [24] M. Mishra, P. M. J. Trevelyan, C. Almarcha, and A. De Wit, *Phys. Rev. Lett.* **105**, 204501 (2010).
  - [25] M. Mishra, M. Martin, and A. De Wit, *Phys. Rev. E* **78**, 066306 (2008).
  - [26] L. Snyder and J. Kirkland, *Introduction to Modern Liquid Chromatography* (Wiley, New York, 1979).
  - [27] M. Martin and G. Guiochon, *J. Chromatogr. A* **151**, 267 (1978).
  - [28] A. Watson and A. Poirson, *J. Opt. Soc. Am. A* **3**, 2001 (1986).
  - [29] M. Islam and J. Azaiez, *Int. J. Numer. Methods Fluids* **47**, 161 (2005).
  - [30] M. N. Islamt, M.S. thesis, University of Calgary, 2003.
  - [31] A. Tartakovsky, *Stochastic Environ. Res. Risk Assess.* **24**, 993 (2010).
  - [32] A. Arya, T. Hewett, R. Larson, and L. Lake, *SPE Reservoir Eng.* **3**, 139 (1988).
  - [33] C. Tan and G. Homsy, *Phys. Fluids* **29**, 3549 (1986).
  - [34] W. Shu, *SPE Journal* **24**, 277 (1984).
  - [35] R. Gharbi, E. Peters, and A. Elkamel, *Energy Fuels* **12**, 801 (1998).
  - [36] U. G. Araktingi and F. M. Orr, Jr., *SPE Adv. Technol. Ser.* **1**, 39 (1990).
  - [37] W. Zimmerman and G. Homsy, *Phys. Fluids A* **3**, 1859 (1991).
  - [38] K. Ghesmat and J. Azaiez, *Transp. Porous Media* **73**, 297 (2008).
  - [39] A. Coutinho and J. Alves, *Comput. Mech.* **23**, 108 (1999).
  - [40] M. A. Cala and R. A. Greenkorn, *Water Resour. Res.* **22**, 919 (1986).
  - [41] J. Bear and Y. Bachmat, *Introduction to Modeling of Transport Phenomena in Porous Media*, Vol. 4 of Theory and Applications of Transport in Porous Media (Kluwer Academic, Dordrecht, 1990).
  - [42] D. Horvath, S. Toth, and A. Toth, *Phys. Rev. Lett.* **97**, 194501 (2006).
  - [43] M. Sajjadi and J. Azaiez, *Can. J. Chem. Eng.* **91**, 687 (2013).
  - [44] F. Furtado and F. Pereira, *Comput. Appl. Math.* **17**, 237 (1998).